Ferromagnetism and lattice distortions in the perovskite $YTiO_3$

W. Knafo,[1,2,3] C. Meingast,[1] A. V. Boris,[4,5] P. Popovich,[4] N. N. Kovaleva,[4,5] P. Yordanov,[4] A. Maljuk,[4,6] R. K. Kremer,[4] H. v. Löhneysen,[1,2] and B. Keimer[4]

[1]*Forschungszentrum Karlsruhe, Institut für Festkörperphysik, D-76021 Karlsruhe, Germany*

[2]*Physikalisches Institut, Universität Karlsruhe, D-76128 Karlsruhe, Germany*

[3]*Laboratoire National des Champs Magnétiques Intenses, UPR 3228, CNRS-UJF-UPS-INSA, 143 Avenue de Rangueil, 31400 Toulouse, Cedex 4, France*

[4]*Max-Planck-Institut für Festkörperforschung, Heisenbergstraße 1, 70569 Stuttgart, Germany*

[5]*Department of Physics, Loughborough University, Leicestershire LE11 3TU, United Kingdom*

[6]*Hahn-Meitner-Institut, Glienicker Strasse 100, 14109 Berlin, Germany*

(Received 8 December 2008; revised manuscript received 30 January 2009; published 26 February 2009)

The thermodynamic properties of the ferromagnetic perovskite $YTiO_3$ are investigated by thermal expansion, magnetostriction, specific-heat, and magnetization measurements. The low-temperature spin-wave contribution to the specific heat, as well as an Arrott plot of the magnetization in the vicinity of the Curie temperature $T_C \simeq 27$ K, is consistent with a three-dimensional Heisenberg model of ferromagnetism. However, a magnetic contribution to the thermal expansion persists well above T_C, which contrasts with typical three-dimensional Heisenberg ferromagnets, as shown by a comparison with the corresponding model system EuS. The pressure dependences of T_C and of the spontaneous moment M_s are extracted using thermodynamic relationships. They indicate that ferromagnetism is strengthened by uniaxial pressures $\mathbf{p} \| \mathbf{a}$ and is weakened by uniaxial pressures $\mathbf{p} \| \mathbf{b}, \mathbf{c}$ and hydrostatic pressure. Our results show that the distortion along the a and b axes is further increased by the magnetic transition, confirming that ferromagnetism is favored by a large $GdFeO_3$-type distortion. The c-axis results, however, do not fit into this simple picture, which may be explained by an additional magnetoelastic effect, possibly related to a Jahn-Teller distortion.

DOI: 10.1103/PhysRevB.79.054431 PACS number(s): 75.30.−m, 75.50.Dd, 75.50.Ee, 75.80.+q

I. INTRODUCTION

ABO_3 perovskites exhibit a large variety of electronic and magnetic properties.[1] The titanate family $ATiO_3$ recently attracted particular interest since $YTiO_3$ orders ferromagnetically below the Curie temperature $T_C \simeq 27$ K, whereas $LaTiO_3$ orders antiferromagnetically below the Néel temperature $T_N \simeq 150$ K.[1–6] In these systems, the $S=1/2$ spins localized on the Ti^{3+} ions are responsible for the magnetic properties. A change from ferromagnetism to antiferromagnetism can be continuously tuned by varying the lanthanum concentration x in the alloys $Y_{1-x}La_xTiO_3$ or by changing the lanthanide A ($A=$Yb$\rightarrow$La) in the undoped $ATiO_3$.[1–4] A $GdFeO_3$-type distortion is driven by ion-size mismatch and comprises rotations of the TiO_6 octahedra. It is responsible for the distorted structure of the $ATiO_3$ crystals, with the space group *Pbnm*. This distortion is more pronounced in $YTiO_3$ than in $LaTiO_3$, and is favored by smaller A^{3+} ions ($A=$Y,La).[4,5] In $YTiO_3$, an additional elongation, by about 3%, of the TiO_6 octahedra is observed. This distortion has been ascribed to staggered ordering of the t_{2g} orbitals (Ti^{3+} ions).[6–8] The switch from antiferromagnetism to ferromagnetism in the $ATiO_3$ perovskites is probably controlled by the extreme sensitivity of the magnetic superexchange interactions to the distortions of the lattice.[4,5,9] However, the mechanism driving this transition is still a matter of considerable debate.[5–13] For a proper description of the magnetic properties, it is thus crucial to carefully consider their dependence on the lattice distortion.

In this paper, we present a study of the thermodynamic properties of $YTiO_3$. Experimental details will be given in Sec. II. In Sec. III, the specific-heat, thermal expansion, magnetization, and magnetostriction data measured with magnetic fields applied along the easy c axis will be presented. In Sec. IV, these results will be discussed and compared to the behavior expected within a three-dimensional (3D) Heisenberg ferromagnetic model.[14] As a specific example, we will show data on the typical 3D Heisenberg system EuS.[15,16] In Sec. V, the relation between the distortion and the magnetic properties will be discussed in the light of our results. The dependence of the distortion on the A^{3+} ionic sizes, on uniaxial pressures, and on the temperature will be considered.

II. EXPERIMENTAL DETAILS

Single crystals of $YTiO_3$ were prepared by the floating-zone method using a four-mirror-type infrared image furnace from the Crystal System Corporation. More details about the crystal growth are given in Ref. 17. Two samples have been investigated and the measurements presented here were obtained on the sample with the sharpest transition at T_C. This sample was cut so that its faces are perpendicular to the a, b, and c axes, its dimensions at room temperature equal to $L_a^0 \simeq 2$ mm, $L_b^0 \simeq 4$ mm, and $L_c^0 \simeq 3$ mm along a, b, and c, respectively, with a mass of 116 mg. Thermal expansion and magnetostriction were measured using a homemade high-resolution capacitive dilatometer,[18,19] with temperature and field sweep rates of 20 mK/s and 0.5 T/min, respectively. Three sets of measurements were performed, where the length L_i was measured along the a, b, and c axes ($i=a$, b, and c, respectively). Specific heat and magnetization were

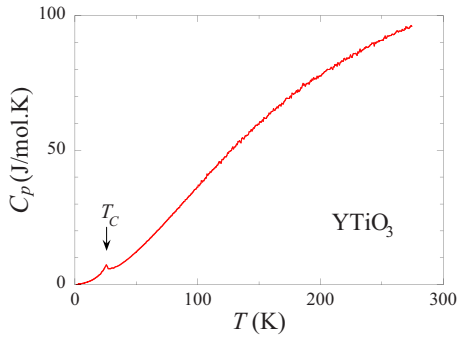

FIG. 1. (Color online) Variation with T of the specific heat C_p of $YTiO_3$.

measured using a physical properties measurement system and a magnetic properties measurement system, respectively (Quantum Design). For all measurements, the magnetic field **H** was applied parallel to the easy axis **c**. The thermal expansion of EuS was measured using a 8-mm-long single crystal grown from the melt by K. Fischer[20] at the Forschungszentrum Jülich, as described elsewhere.

III. RESULTS

A. Specific heat and thermal expansion

In Fig. 1, the specific heat C_p of $YTiO_3$ is shown in a C_p versus T plot. Ferromagnetic ordering is characterized by an anomaly at $T_C=26.8\pm0.3$ K, defined at the minimum of the slope of $C_p(T)$. In Fig. 2(a), the variation with T of the relative lengths $\Delta L_i/L_i$ is shown for $i=a$, b, and c, with $\Delta L_i/L_i$ being fixed to zero at room temperature. The linear thermal expansion coefficients $\alpha_i=(1/L_i)\partial L_i/\partial T$ with $i=a$, b, and c are extracted from these data and are plotted in Fig. 2(b). The volume change $\Delta V/V=\Sigma_{i=a,b,c}\Delta L_i/L_i$ and the related volume

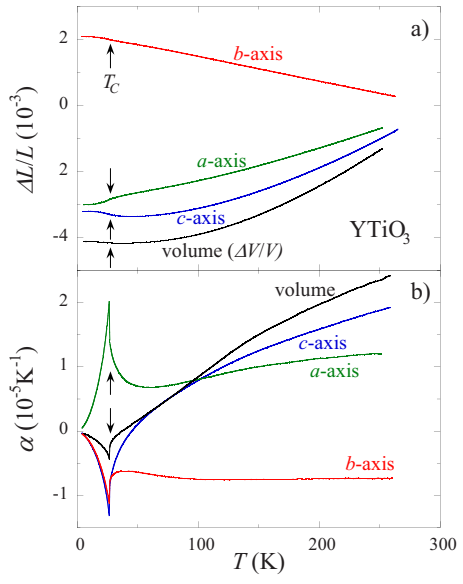

FIG. 2. (Color online) Variation with T (a) of the relative lengths $\Delta L_i/L_i$ for $i=a$, b, and c and of the relative volume $\Delta V/V$ and (b) of the thermal expansion coefficients α_i for $i=a$, b, c, and V.

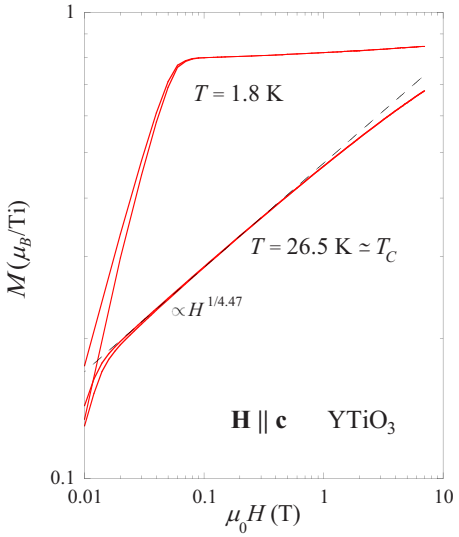

FIG. 3. (Color online) Field dependence of the magnetization M, on a log-log scale, at $T=1.8$ K and $T=26.5$ K $\simeq T_C$.

thermal expansion coefficient $\alpha_V=(1/V)\partial V/\partial T$ are also shown in Figs. 2(a) and 2(b), respectively. As seen in Fig. 2, changes of slope in L_a, L_b, L_c, and V are induced at T_C, leading to a positive anomaly in α_a and to negative anomalies in α_b, α_c, and α_V. The volume decrease below T_C, which is similar to the invar effect, will be further related to the negative hydrostatic pressure dependence of T_C. From the thermal expansion data, we extract a Curie temperature $T_C=26.8\pm0.05$ K at the extremum of the slope of $\alpha_i(T)$. This is in good agreement with prior observations.[17] At temperatures sufficiently higher than T_C, L_a, L_c, and V increase with T, while L_b decreases with T [Fig. 2(a)]. This leads to the positive values of α_a, α_c, and α_V and to the negative values of α_b observed at high temperatures in Fig. 2(b). The anisotropy of α_i at high temperatures is a consequence of the lattice distortions, which will be discussed in Sec. V.

B. Magnetization and magnetostriction

In Fig. 3, the magnetization versus field $M(H)$ is shown for $\mathbf{H}\|\mathbf{c}$ in a log-log plot, at $T=1.8$ K and $T=26.5$ K $\simeq T_C$. At $T=1.8$ K, a linear increase in $M(H)$ is obtained for $\mu_0 H<\mu_0 H^*\simeq0.06$ T and is related to the alignment of ferromagnetic domains. For $H>H^*$, the spins are aligned parallel to **H** and the magnetization M reaches $M_s\simeq0.8\mu_B$. In this regime, a slight increase in $M(H)$ is observed. Indeed, M_s is not yet fully saturated and is somewhat smaller than the full moment of μ_B expected for the $S=1/2$ Ti^{3+} ions.[14,21] At $T\simeq T_C$, M increases first almost linearly with H, for $\mu_0 H<\mu_0 H^{*\prime}\simeq0.02$ T, and then varies as $M\propto H^{1/\delta}$, with $\delta=4.47\pm0.2$, for $\mu_0 H^{*\prime}<\mu_0 H<1$ T. This power law, observed above 1 T, is characteristic of the critical ferromagnetic regime. Deviations are observed when M becomes close to M_s.

In Ref. 17, low-temperature magnetization measurements were reported on the same sample as in the present work and moments of $0.84\mu_B$ and $0.82\mu_B$ were found for a magnetic field of 7 T applied along **b** and **c**, respectively. These data

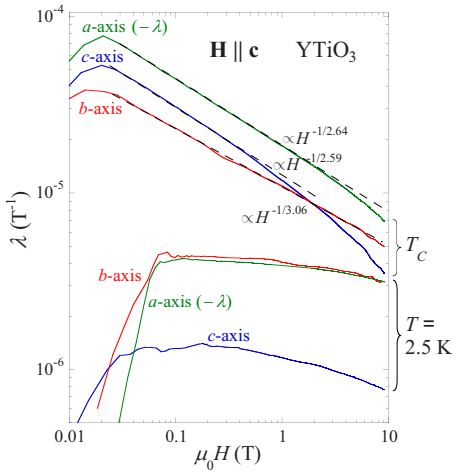

FIG. 4. (Color online) Field dependence of the magnetostriction λ_i, on a log-log scale, for $i=a$, b, and c at $T=2.5$ K and $T_C=26.7$ K (λ_a is plotted with a minus sign).

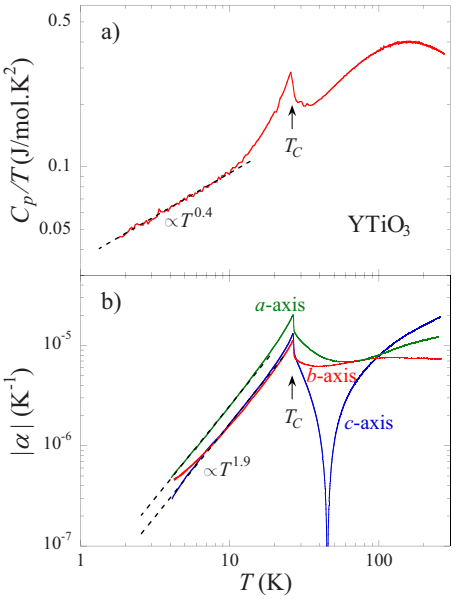

FIG. 5. (Color online) (a) Specific heat and (b) thermal expansion of $YTiO_3$ in C_p/T and $|\alpha_i|$ versus T on log-log scales, respectively.

agree well with the saturated magnetic moment of $0.84\mu_B$ reported in Refs. 21 and 22 and with the moments of $(0.83\pm0.05)\mu_B$ and $(0.84\pm0.05)\mu_B$, for the a and c axes, respectively, determined by recent magnetic Compton profile experiments.[23]

In Fig. 4, the magnetostriction coefficients $\lambda_i=(1/L_i)\partial L_i/\partial(\mu_0 H)$ are plotted as a function of H on a log-log scale, at $T=2.5$ K and $T_C=26.7$ K, with $i=a$, b, and c, and $\mathbf{H}\|\mathbf{c}$. For all temperatures and magnetic fields, λ_b and λ_c are positive while λ_a is negative. For the three configurations at $T=2.5$ K, $|\lambda_i(H)|$ increases for $\mu_0 H<\mu_0 H^*\simeq 0.06$ T and is almost constant for $H>H^*$ when the domains are aligned. At T_C, $|\lambda_i(H)|$ increases before reaching a maximum at $\mu_0 H^{*\prime}\simeq 0.02$ T. For $\mu_0 H>\mu_0 H^{*\prime}$, a critical regime is observed, where $|\lambda_i(H)|\propto H^{-1/\delta_i'}$, with $\delta_i'=2.64$, 3.06, and 2.59 ± 0.1 for $i=a$, b, and c, respectively. While the power law is followed up to almost 10 T in λ_b, deviations are found for $\mu_0 H>1$ T in λ_a and λ_c.

IV. FERROMAGNETIC PROPERTIES

A. Low-temperature spin waves

In Fig. 5(a), the specific heat of $YTiO_3$ is plotted in a log-log plot of C_p/T versus T. Well below T_C, the phonon contribution can be neglected and the signal, which varies as $C_p(T)\propto T^{1.4}$ up to 10 K, is believed to be only magnetic. This power law is compatible with isotropic 3D Heisenberg ferromagnetic spin waves, for which a $T^{1.5}$ law would be expected, and is thus in good agreement with the spin-wave dispersion observed by neutron scattering.[14] The slight deviation from the $T^{1.5}$ law might result from a small spatial anisotropy of the exchange, with the spin-wave contribution to the specific heat of a ferromagnet varying as $C_p(T)\propto T^{d/2}$, where d is the dimensionality of the exchange. It may also be related to possible additional antiferromagnetic spin fluctuations and/or to spin anisotropies originating from spin-orbit coupling (see below).

In Fig. 5(b), the thermal expansion is plotted in a log-log plot of $|\alpha_i|$ versus T, for $i=a$, b, and c. Power laws $\alpha_i\propto T^{1.9}$ are found up to almost 20 K for $i=a$ and c, while no clear power law is observed for $i=b$. As simple 3D Heisenberg ferromagnetic spin waves should lead to $\alpha_i\propto C_p\propto T^{1.5}$, the different T dependences of C_p and α_i reported here may result from anisotropic exchange interactions, which lead to weak additional magnetic Bragg reflections due to canting of the ferromagnetic moments.[14] Weak low-energy spin fluctuations around these wave vectors may contribute to the deviation of the temperature dependence of the low-temperature specific heat and thermal expansion from the predictions of a simple ferromagnetic Heisenberg model.[24] Further studies of the spin-wave spectra (e.g., by neutron scattering) and detailed calculations are needed for a quantitative explanation of the results obtained here. Systematic studies by specific heat and thermal expansion of the $ATiO_3$ family, such as the work initiated in Ref. 6, may be of importance to understand the evolution of the low-temperature magnetic properties.

B. Arrott plot and critical fluctuations

To analyze the critical ferromagnetic regime, the magnetization was measured as M versus H at several temperatures close to T_C. In Fig. 6, an Arrott plot of these data is shown as $M^{1/\beta}$ versus $(H/M)^{1/\gamma}$ for $25.9\leq T\leq 27.1$ K. The critical exponents $\beta=0.392\pm0.05$ and $\gamma=1.475\pm0.1$ used in this plot were determined from a fit of $M(H,T)$ using Arrott's equation of state[25,26]

$$M^{1/\beta}=c_1\left(\frac{H}{M}\right)^{1/\gamma}-c_2(T-T_C) \qquad (1)$$

for $0.02<\mu_0 H<1.3$ T and $25.9\leq T\leq 27.1$ K. The value of $T_C=26.44\pm0.05$ K obtained from this fit agrees well with that obtained from the specific heat and thermal expansion (Sec. III A). From Eq. (1),

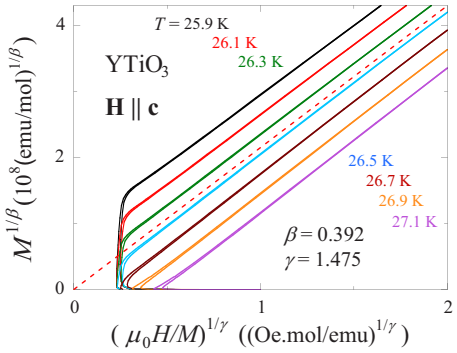

FIG. 6. (Color online) Best Arrott plot of the data, with $\beta=0.392$, $\gamma=1.475$, and $T_C=26.44$ K. The dotted line indicates the critical regime at T_C associated with the exponent $\delta=4.76$.

$$M(H,T_C) \propto H^{1/\delta}, \tag{2}$$

with

$$\delta = (\beta+\gamma)/\beta. \tag{3}$$

Using the exponents α and β obtained with Arrott's method, we calculate the critical exponent $\delta=4.76\pm0.2$, which agrees favorably with $\delta=4.47\pm0.2$ directly obtained from the fit by a power law of $M(H)$ at 26.5 K (Sec. III B).

In Table I, the exponents β, γ, and δ expected for different classes of universality[27] are listed for comparison. The exponents extracted from the Arrott plot of the magnetization of $YTiO_3$ are rather close to those of the 3D Heisenberg universality class and, to a lesser degree, to the exponents expected for the 3D *XY* and 3D Ising universality classes. A similar plot was made in Ref. 28 using 3D Heisenberg exponents but without a preliminary fit of the $M(H,T)$ data as done here. As already inferred from the behavior of the low-temperature spin waves, the critical behavior of the magnetization, too, is thus consistent with a 3D Heisenberg picture of ferromagnetism (cf. Sec. IV A and Ref. 14).

In the following, the power laws reported for the magnetostriction at T_C (Fig. 4) are related to the critical power law of the magnetization (Fig. 3) and to the critical exponents α and β. Using the Maxwell relation

$$\lambda_i = \frac{1}{L_i}\frac{\partial L_i}{\partial(\mu_0 H)} = -\frac{\partial M}{\partial p_i}, \tag{4}$$

the magnetostriction coefficients can be expressed as functions of the uniaxial pressure dependences of the magnetization. Assuming that $\partial c_1/\partial p_i=0$, the derivative of Eq. (1) leads to, at $T=T_C$,

$$\lambda_i(H,T_C) = -A\frac{\partial T_C}{\partial p_i}H^{-1/\delta'}, \tag{5}$$

with

$$A = c_1^{-\gamma/\delta'}c_2\gamma/\delta, \quad \delta' = (\beta+\gamma)/(1-\beta). \tag{6}$$

From the exponents α and β obtained by the Arrott fit of the magnetization, a critical exponent $\delta'=3.07\pm0.5$ is expected to characterize the magnetostriction at T_C. This value is in good agreement with the values $2.59\leq\delta_i'\leq3.06$ determined from the fits of $\lambda_i(H)$ at T_C (see Sec. III B). For each set of (β,γ), the corresponding δ' values are also given in Table I. These values are compatible with a 3D Heisenberg scenario of ferromagnetism for $YTiO_3$ associated with $\delta'=2.77$. The slight variations of δ_i' with i are not understood and may result from various secondary effects (anisotropic energy scales, defects, etc.).

To our knowledge, $YTiO_3$ is the second ferromagnetic system known, after the itinerant ferromagnet UIr,[29] where a critical power law is reported in the magnetostriction at T_C. We believe that such an effect is quite general and should be present in most ferromagnets, once the field and temperature ranges are properly chosen. We note that, more than 60 years ago, Belov[30] had theoretically predicted a similar law, but only within a mean-field approach, which corresponds to $\beta=0.5$, $\gamma=1$, and $\delta=\delta'=3$ (cf. Table I). Our approach is more general and permits one to obtain the critical exponent δ' for each combination of (β,γ) and thus for each universality class.

TABLE I. Critical exponents β, γ, δ, and δ' obtained here for $YTiO_3$ and expected for different universality classes (Ref. 27).

Critical exponents	β	γ	δ	δ'
$YTiO_3$: best fit	0.392(50)	1.475(100)	4.76(20)	3.07(50)
3D Heisenberg	0.367	1.388	4.78	2.77
3D *XY*	0.345	1.316	4.81	2.54
3D Ising	0.326	1.238	4.80	2.32
2D Ising	0.125	1.75	15	2.14
Mean field	0.5	1	3	3

C. High-temperature magnetic signal: Deviation from a pure 3D Heisenberg ferromagnet

The distortion of the lattice induces the strong anisotropy observed in the high-temperature thermal expansion of $YTiO_3$ (see Fig. 2). This anisotropic lattice signal must be properly taken into account to extract the magnetic contribution to the thermal expansion. Since α_a and α_c are rather close above 100 K, we assume that the lattice contributions to α_a and α_c are similar, so that $\Delta\alpha=\alpha_a-\alpha_c$, which is plotted in Fig. 7(a), can be considered as a signal representative of the magnetic thermal expansion. In this plot, the dashed red line is a guide to the eyes indicating the "remaining" nonmagnetic background and the yellow area corresponds to the estimated magnetic contribution. In Fig. 7(b), the thermal expansion α of cubic EuS,[31] which is known as a prototype of 3D Heisenberg ferromagnetism,[32–34] is shown for comparison. The dashed blue line is a guide to the eyes indicating the nonmagnetic background and the magnetic contribution is estimated by the blue area. The estimates of the magnetic contribution to the thermal expansion of $YTiO_3$ and EuS are plotted in Fig. 7(c). In this plot, the magnetic thermal expansion coefficient α^{mag} is normalized by its maximal value $\alpha^{\mathrm{mag}}_{\mathrm{max}}$ and the temperature T is normalized by T_C. Figure 7(c) indicates that, in $YTiO_3$, the magnetic signal has a significant weight above T_C and extends up to about $5T_C$ while, in EuS,

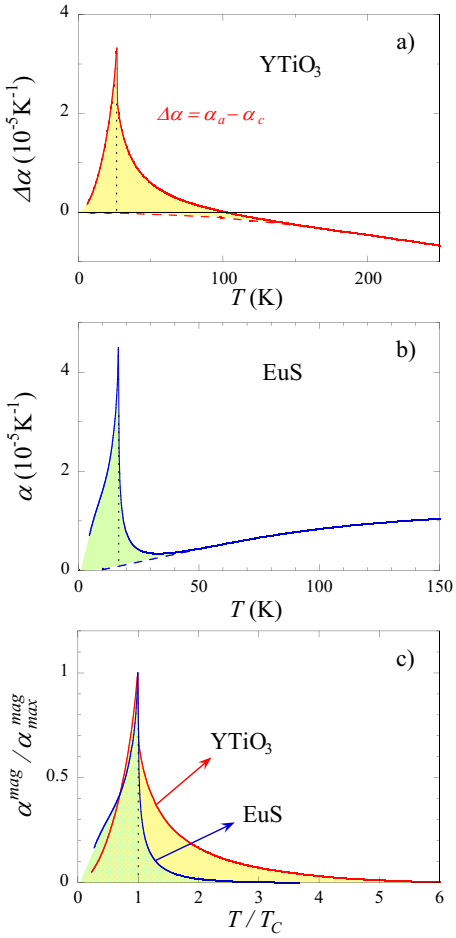

FIG. 7. (Color online) Temperature dependence (a) of $(\Delta\alpha = \alpha_a - \alpha_c)$ for $YTiO_3$ and (b) of α for EuS. In both plots, the dashed line is a guide to the eyes indicating the nonmagnetic background; the shaded (colored) area is the magnetic contribution deduced from the raw data after subtraction of this background and the vertical dotted line indicates the ferromagnetic transition temperature. (c) Magnetic contribution to the thermal expansion estimated for $YTiO_3$ (red line) and for EuS (blue line) in a normalized $\alpha^{mag}/\alpha^{mag}_{max}$ vs T/T_C plot.

it has most of its intensity below T_C and vanishes completely above about $2T_C$. Thus, the magnetic fluctuations of $YTiO_3$ cannot be described as those of a simple 3D Heisenberg ferromagnet.

As shown in the inset of Fig. 8, the specific heat $C_p(T)$ and the volume thermal expansion $\alpha_V(T)$ can be scaled at high temperatures using an empirical parameter $y=3.96 \times 10^{-6}$ mJ/mol defined by $C_p = y\alpha_V$. Assuming that the magnetic contribution to C_p and α_V is negligible above 200 K, and that there is a single Gruneisen parameter associated with the phonons for the [0,300 K] range, we can estimate the phonon contribution to the specific heat by $C_p^{ph} = C_p - z(C_p - y\alpha_V)$, with $z=0.2$ being adjusted, so that no anomaly remains at T_C. The main frame of Fig. 8 shows the resulting estimate of the magnetic contribution $C_p^{mag}(T)$ to the specific heat. This plot confirms the conclusions from Fig. 7, i.e., a magnetic contribution is present up to more than 100 K. Integration of the estimated magnetic heat capacity leads to the magnetic entropy $\Delta S^{mag} \simeq 4.5$ J/mol K. This entropy is

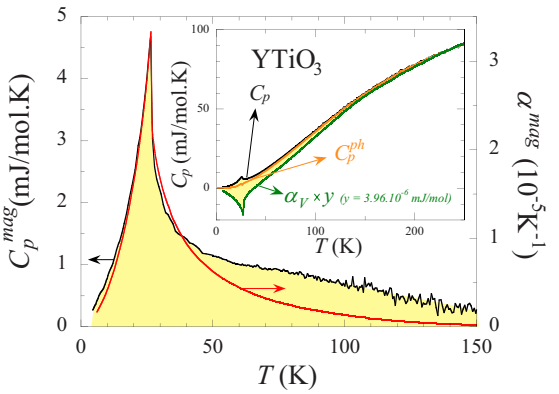

FIG. 8. (Color online) Temperature dependence of the magnetic contribution C_p^{mag} to the specific heat in a C_p^{mag}/T versus T plot. The inset shows the scaling of $C_p(T)$ (red line) and $\alpha_V(T)$ (green line), which permitted us to estimate the nonmagnetic contribution (blue line).

roughly equal to the full spin entropy $\Delta S^{mag}_{full} = R \ln 2 \simeq 5.8$ J/mol K expected for the $S=1/2$ spin system; the fact that ΔS^{mag} is about 20% smaller than ΔS^{mag}_{full} may be imputed to the experimental error.

In Fig. 8, the estimated magnetic contributions to the thermal expansion $\alpha^{mag}(T)$ and to the specific heat $C_p^{mag}(T)$ are plotted together. While the two quantities vary similarly below 50 K, their shapes become quite different above 50 K; this indicates the limits of the two methods used here to estimate the nonmagnetic background. The comparison of both plots permits us to conclude that the magnetic signal extends up to $(5 \pm 1)T_C$. In spite of the uncertainty, Figs. 7(c) and 8 show a clear deviation in $YTiO_3$ from the behavior of the prototypical 3D Heisenberg ferromagnet EuS. The origin of this deviation is not yet understood. In principle, a modified conventional spin-only fluctuation model, for example, with competing (and possibly low-dimensional, see Refs. 35–37) antiferromagnetic and ferromagnetic interactions could describe this anomalously high-temperature magnetic signal. However, this is in apparent contradiction with the magnon spectra reported by neutron scattering, which do not exhibit pronounced deviations from the predictions of a 3D Heisenberg model with nearest-neighbor interactions.[14] An alternative explanation of the extended magnetic fluctuation regime could be offered by spin-orbital fluctuations models, where an energy scale significantly exceeding the magnon bandwidth (in Refs. 38 and 39, orbital fluctuations were associated with an excitation at about 250 meV), could actuate ferromagnetic fluctuations at temperatures between T_C and room temperature.[11] Further work is required to ascertain whether a quantitatively consistent picture of the spin[14] and orbital[38,39] excitation spectra and thermodynamics of $YTiO_3$ can be obtained.

V. COUPLING BETWEEN THE LATTICE AND THE MAGNETIC PROPERTIES

A. Uniaxial pressure dependences: Comparison with $LaTiO_3$

Figure 9 shows the anomalies at T_C in the specific heat and in the thermal expansion of $YTiO_3$. These anomalies are

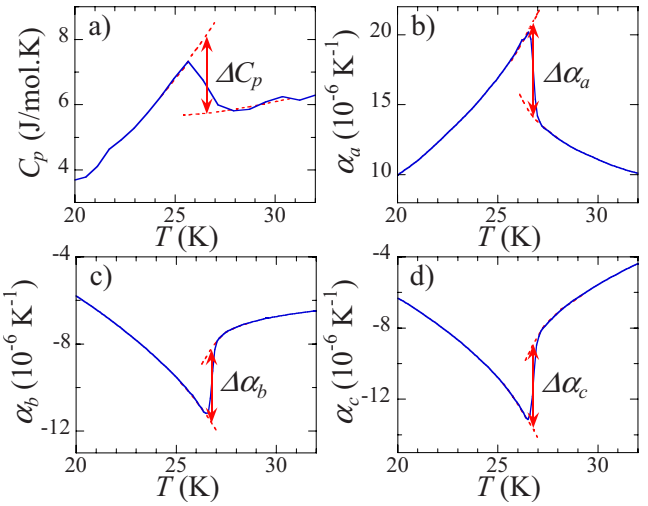

FIG. 9. (Color online) Ferromagnetic ordering anomaly (a) in the specific heat and (b)–(d) in the thermal expansivity coefficients along a, b, and c. In these curves, the jumps ΔC_p, $\Delta\alpha_a$, $\Delta\alpha_b$, and $\Delta\alpha_c$ at the ferromagnetic ordering are indicated by arrows.

typical of a second-order phase transition, whose jumps are estimated as $\Delta C_p = 2.3 \pm 0.1$ J/mol K in the specific heat and as $\Delta\alpha_a = (6.6 \pm 0.3) \times 10^{-6}$ K^{-1}, $\Delta\alpha_b = (-3.4 \pm 0.2) \times 10^{-6}$ K^{-1}, and $\Delta\alpha_c = (-4.7 \pm 0.2) \times 10^{-6}$ K^{-1} in the thermal expansion. Using the Ehrenfest relation

$$\frac{\partial T_C}{\partial p_i} = \frac{\Delta\alpha_i V_m T_C}{\Delta C_p}, \tag{7}$$

where $V_m = 3.46 \times 10^{-5}$ m^3/mol is the molar volume and p_i is a uniaxial pressure applied along i ($i=a$, b, and c), we extract the uniaxial pressure dependences $\partial T_C/\partial p_i$ reported in Table II. The sum of the three uniaxial pressure dependences of T_C gives the hydrostatic pressure dependence $\partial T_C/\partial p_h = (-6.0 \pm 0.6) \times 10^{-2}$ K/kbar. Assuming that, in $YTiO_3$, $\partial T_C/\partial p_h$ remains constant under hydrostatic pressure, ferromagnetism may be destroyed above $p_c \simeq 400$ kbar.

For comparison, the uniaxial pressure dependences of T_N, for the antiferromagnet $LaTiO_3$, are also listed in Table II. To calculate them, T_C in Eq. (7) was substituted by $T_N \simeq 146$ K, $\Delta C_p = 10$ J/mol K, $\Delta\alpha_a = (-5 \pm 0.5) \times 10^{-5}$ K^{-1}, $\Delta\alpha_b = (5 \pm 0.5) \times 10^{-5}$ K^{-1}, and $\Delta\alpha_c \simeq 0$ being estimated from Ref. 40. While $\partial T_N/\partial p_c$ is too small to be extracted from Ref. 40, $\partial T_N/\partial p_a$ and $\partial T_N/\partial p_b$ are such that $\partial T_N/\partial p_a = -\partial T_N/\partial p_b < 0$. For $\mathbf{p}\|\mathbf{a},\mathbf{b}$, the uniaxial pressure dependences of T_C and T_N, for $YTiO_3$ and $LaTiO_3$, respectively, have thus opposite signs. The effects of pressure along c are such that $\partial T_C/\partial p_c < 0$ and $\partial T_N/\partial p_c \simeq 0$. In Secs. V B and V C, the uniaxial pressure dependences of T_C and T_N in $YTiO_3$ and $LaTiO_3$, respectively, will be interpreted as resulting from pressure-induced modifications of the distortion.

TABLE II. Uniaxial and hydrostatic pressure dependences of T_C and M_s for $YTiO_3$ and of T_N for $LaTiO_3$. The ratio ρ_i of the pressure dependences of T_C and M_s is given for $YTiO_3$.

	$YTiO_3$			$LaTiO_3$
	$\partial \ln T_C/\partial p_i$ (10^{-3} kbar^{-1})	$\partial \ln M_s/\partial p_i$ (10^{-3} kbar^{-1})	ρ_i	$\partial \ln T_N/\partial p_i$ (10^{-2} kbar^{-1})
p_a	9.9 ± 1.0	2.7 ± 0.4	3.7 ± 1.0	-1.9 ± 0.4
p_b	-5.1 ± 0.5	-2.7 ± 0.4	1.9 ± 0.5	1.9 ± 0.4
p_c	-7.1 ± 0.7	-0.77 ± 0.15	9.1 ± 2.5	$\simeq 0$
p_h	-2.3 ± 0.3	-0.77 ± 0.15	2.9 ± 1.0	$\simeq 0$

Well below T_C and for $\mu_0 H > \mu_0 H^* = 0.06$ T, $M \simeq M_s \simeq 0.8\mu_B$ (Fig. 3) and the magnetostriction coefficients of $YTiO_3$ are almost constant, having the values $\lambda_a \simeq (-3.5 \pm 0.5) \times 10^{-6}$ T^{-1}, $\lambda_b \simeq (3.5 \pm 0.5) \times 10^{-6}$ T^{-1}, and $\lambda_c \simeq (1.0 \pm 0.2) \times 10^{-6}$ T^{-1} (Fig. 4). Using the Maxwell relation given in Eq. (4), we extract

$$\frac{\partial M_s}{\partial p_i} = -\lambda_i (T = 2.5 \text{ K}). \tag{8}$$

The values of $\partial M_s/\partial p_i$, for $i=a$, b, and c, as well as their sum, the hydrostatic pressure dependence $\partial M_s/\partial p_h$, are summarized in Table II.

For each $i=a$, b, c, and h ($h \leftrightarrow$ hydrostatic), the pressure dependences $\partial T_C/\partial p_i$ and $\partial M_s/\partial p_i$ have always the same sign, being both positive for $i=a$ and both negative for $i=b,c,h$ (Table II). Ferromagnetic order is thus stabilized by uniaxial pressure $\mathbf{p}\|\mathbf{a}$ and is destabilized by uniaxial pressure $\mathbf{p}\|\mathbf{b},\mathbf{c}$ and by hydrostatic pressure. Consequently, the ratio ρ_i, defined by

$$\rho_i = \frac{M_s}{T_C} \frac{\partial T_C/\partial p_i}{\partial M_s/\partial p_i} \tag{9}$$

is always positive. As shown in Table II, we find that ρ_i is strongly anisotropic, being bigger when the i axis is easier (c=easy, a=intermediate, and b=hard [17,21]).

Although $YTiO_3$ is a localized ferromagnet, its saturated moment, at about 5 T, is only 80% of the fully saturated moment $M_s^{\text{full}} = 1\mu_B$. A small canted antiferromagnetic moment $M_{\text{AF}} \approx 0.1\mu_B$ was reported by neutron scattering in $YTiO_3$ (Ref. 14) and explained partly why M_s is reduced. In addition, the reduction in M_s may indicate an enhanced phase space for quantum magnetic fluctuations. The question is whether this reduction comes from usual spin-only fluctuations or if it results from more complicated fluctuations involving orbital degrees of freedom.[11,14] The high values of $\partial M_s/\partial p_i$ in $YTiO_3$ may result from the combination of two effects, which can be summarized as the uniaxial pressure-induced transfers of weight (i) between the ferromagnetic moment M_s and the antiferromagnetic moment M_{AF} and (ii) between M_s and some quantum magnetic fluctuations δM. The second effect is similar to what happens in itinerant ferromagnets, where M_s is reduced by quantum fluctuations δM of the magnetic moment, and where the strong pressure dependences of M_s are related to those of δM.

A similar analysis as the one presented here was reported for the itinerant weak ferromagnet UIr (Ref. 29) in the framework of the Moriya spin fluctuation theory of itinerant magnetism.[41,42] By analogy, a spin fluctuation theory, adapted to the particular case of $YTiO_3$, may be appropriate.

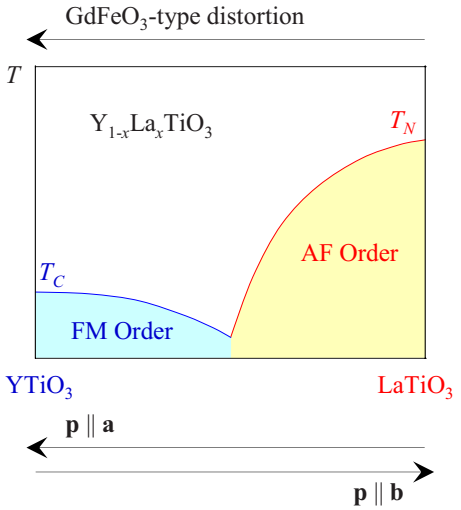

FIG. 10. (Color online) Schematic magnetic phase diagram of $Y_{1-x}La_xTiO_3$ (AF=antiferromagnetic and FM=ferromagnetic). The arrows indicate the effects of increasing the $GdFeO_3$-type distortion and of applying uniaxial pressures $\mathbf{p}\|\mathbf{a},\mathbf{b}$.

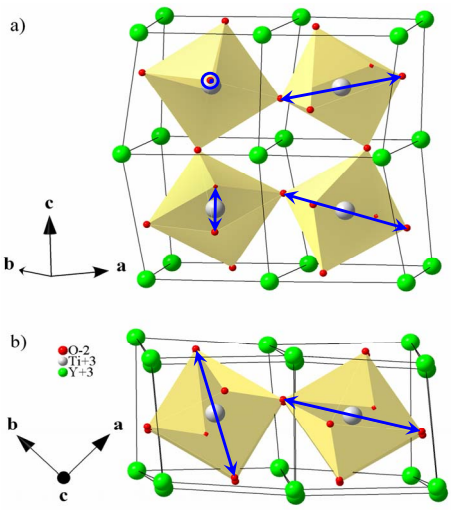

FIG. 11. (Color online) Schematics of the lattice structure of $YTiO_3$. The Ti^{3+} ions are represented by gray spheres, the Y^{3+} ions by green spheres, and the O^{2-} ions by red spheres. The TiO_6 octahedra are colored in yellow, and blue arrows show their elongated direction, possibly due to the Jahn-Teller distortion.

B. Coupling between the $GdFeO_3$-type distortion and the magnetic ordering

In the $ATiO_3$ perovskites, the $GdFeO_3$-type distortion comprises a combination of tilts and rotations of the TiO_6 octaedra. This results in an orthorhombic structure, where $b>a_0\sqrt{2}>c/\sqrt{2}>a$, with a_0 being the lattice parameter of an undistorted cubic structure.[43,44] In the alloys $Y_{1-x}La_xTiO_3$, La substitution induces a decrease in the $GdFeO_3$-type distortion, which is believed to control the change from ferromagnetism to antiferromagnetism[1–5] (Fig. 10). This picture, in which ferromagnetism is favored by a large $GdFeO_3$-type distortion, is qualitatively confirmed by the increase in the distortion of the (a,b) plane induced below T_C (see Fig. 2). In the following, we will further show that, for $\mathbf{p}\|\mathbf{a},\mathbf{b}$, the uniaxial pressure dependences of T_C and T_N are mainly controlled by those of the $GdFeO_3$-type distortion.

In $YTiO_3$ and $LaTiO_3$, the negative sign of $\partial T_C/\partial p_b$ and the positive sign of $\partial T_N/\partial p_b$ (see Table II), respectively, imply that a uniaxial pressure $\mathbf{p}\|\mathbf{b}$ can be seen as equivalent to La doping (cf. the corresponding arrow in Fig. 10). Conversely, the fact that $\partial T_C/\partial p_a$ is positive while $\partial T_N/\partial p_a$ is negative (Table II) implies that $\mathbf{p}\|\mathbf{a}$ is equivalent to Y doping (see Fig. 10). As $\mathbf{p}\|\mathbf{b}$ induces a compression along b and, because of elasticity, extensions along a and c, its effects are very similar to those of reducing the $GdFeO_3$-type distortion. By analogy, $\mathbf{p}\|\mathbf{a}$ leads to a compression along a and to small extensions along b and c, which is similar to increasing the $GdFeO_3$-type distortion. Thus, we conclude that $\mathbf{p}\|\mathbf{a}$ and $\mathbf{p}\|\mathbf{b}$ induce an increase and a decrease in the $GdFeO_3$-type distortion, respectively, which are responsible for the various signs of $\partial T_{C,N}/\partial p_i$ for $i=a,b$.

The uniaxial pressure dependences of T_C and T_N are a consequence of the high sensitivity of the superexchange interactions to the bond angles between the ions, whose positions are very sensitive to the pressure-induced modifications of the $GdFeO_3$-type distortion. The application of uniaxial pressures $\mathbf{p}\|\mathbf{a},\mathbf{b}$, as well as the variation of the A^{3+} ion, thus permits us to tune the competition between the ferromagnetic and the antiferromagnetic exchange interactions, via a change in the $GdFeO_3$-type distortion.

However, a pressure-driven change in the $GdFeO_3$-type distortion cannot explain the results obtained for $\mathbf{p}\|\mathbf{c}$, i.e., $\partial T_C/\partial p_c<0$ and $\partial T_N/\partial p_c\simeq 0$. Indeed, $\partial T_C/\partial p_c>0$ and $\partial T_N/\partial p_c<0$ would be expected if $\mathbf{p}\|\mathbf{c}$ merely modified the $GdFeO_3$-type distortion (since $\mathbf{p}\|\mathbf{c}$ contracts c, it should increase the $GdFeO_3$-type distortion). Another mechanism, in addition to the $GdFeO_3$-type distortion, is needed to understand the pressure dependences of T_C and T_N for $\mathbf{p}\|\mathbf{c}$. In Sec. V C, we will show that a higher sensitivity of the c-axis length to the intrinsic elongations of the octahedra may be the origin of this behavior.

C. Distortion of the TiO_6 octahedra

1. Microscopic description

The lattice structure of $YTiO_3$ is represented schematically in Fig. 11, where the alternation of tilts and rotations of the TiO_6 octahedra (in yellow) is due to the $GdFeO_3$-type distortion. An additional distortion consists of an elongation of each octahedron along a particular axis (blue arrows in Fig. 11) and of contractions perpendicularly to this axis. In Refs. 4, 5, 7, and 8, the fact that the elongated axes vary from one site to another was ascribed to a staggered ordering of the t_{2g} orbitals (Ti^{3+} ions) via a collective Jahn-Teller effect. By geometrical considerations, we can qualitatively estimate the macroscopic distortion induced by the elongations of the octahedra. As seen in Fig. 11, the elongated axes are almost contained within the (a,b) plane, i.e., perpendicularly to the c axis. This implies that the elongations of the octahedra induce a contraction of the c axis. In the (a,b) plane, the elongated axes of two adjacent octahedra subtend

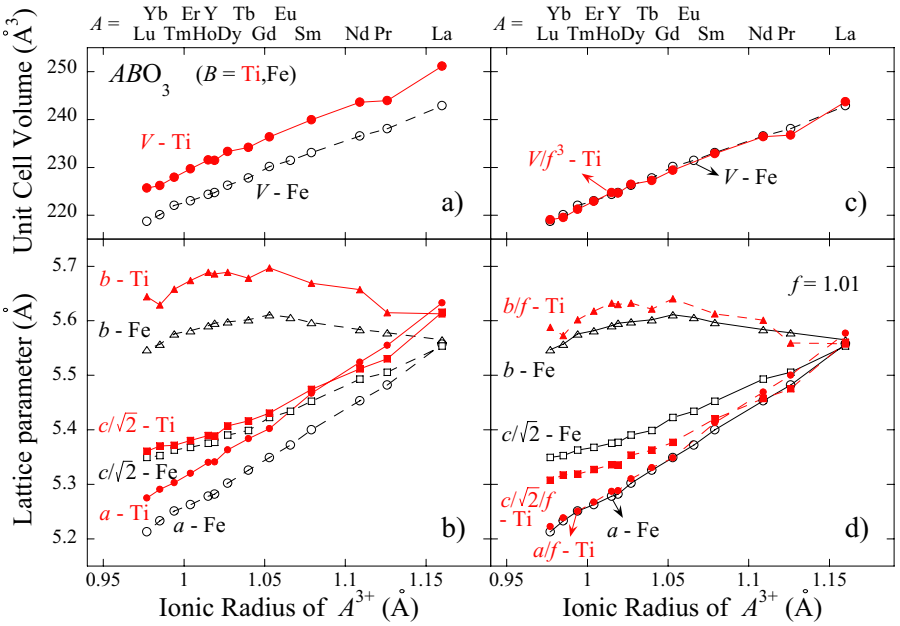

FIG. 12. (Color online) Variations for the $ATiO_3$ and $AFeO_3$ systems of (a) the unit-cell volume V and (b) the lattice parameters a, b, and $c/\sqrt{2}$, as a function of the ionic radius of A^{3+}. In (c) and (d), the volume and the lattice parameters of $ATiO_3$ and $AFeO_3$ are scaled together using the empirical factor $f=1.01$.

an angle of about 60°, so that the elongations and contractions of the different octahedra almost cancel each other. Since the projections of the elongated axes are larger along b than along a (the elongated axes subtend an angle of about 30° with b and of about 60° with a), we finally conclude that the elongations of the octahedra are responsible for a small elongation of b and for a tiny compression of a and, in addition to the main effect, a compression along c.

2. *Lattice parameters: Comparison of the families $ATiO_3$ and $AFeO_3$*

Here we propose a method, based on a comparison of the lattice parameters a, b and c of the families $ATiO_3$ and $AFeO_3$, to confirm the description made in Sec. V C 1 of the effects of the elongation of the octahedra on a, b, and c. Assuming that these elongations are related to a Jahn-Teller distortion,[45,46] the comparison of the lattice parameters of $ATiO_3$ and $AFeO_3$ can be justified by the fact that, contrary to Ti^{3+}, Fe^{3+} is not Jahn-Teller active, so that $AFeO_3$ can be considered as a non-Jahn-Teller reference for $ATiO_3$.

In Figs. 12(a) and 12(b), the unit-cell volume V and the lattice parameters a, b, and $c/\sqrt{2}$ are plotted versus the ionic radius of the A^{3+} ions for several compounds of the families $ATiO_3$ and $AFeO_3$ (A=Lu→La).[10,44,47–49] The ionic radii of the A^{3+} ions are taken from Ref. 49, assuming a number of eight nearest neighbors.[6] While $LaTiO_3$ and $LaFeO_3$ are almost undistorted ($a \simeq b \simeq c/\sqrt{2}$), Fig. 12(b) shows a strong distortion of the pseudocubic lattice in $ATiO_3$ and $AFeO_3$, once A^{3+} is smaller than La^{3+}.

In Fig. 12(c), the unit-cell volumes V^{ATiO_3} of the $ATiO_3$ compounds are scaled empirically with the unit-cell volumes V^{AFeO_3} of the $AFeO_3$ compounds using a scaling factor $f=1.01$ defined by $V^{ATiO_3}=V^{AFeO_3}f^3$. In Fig. 12(d), the lattice parameters of $ATiO_3$ are scaled to those of $AFeO_3$ using the factor $1/f$. As the undistorted limit in the ABO_3 perovskites corresponds to a cubic lattice parameter $a_0^{ABO_3}=2(r_O+r_B)$, where r_O and r_B are the ionic radii of the O^{2-} and B^{3+} ions, respectively, we associate the empirical scaling factor $f=1.01$ to the ratio $a_0^{ATiO_3}/a_0^{AFeO_3}=1.013$ calculated with $r_O=1.35$, $r_{Ti}=0.67$, and $r_{Fe}=0.645$ Å.[49]

Since the ionic radii of Ti^{3+} and Fe^{3+} are very close, we assume that, for the two families, the $GdFeO_3$-type distortion induces similar variations of their lattice parameters in the scaled plot of Fig. 12(d). Consequently, the elongations of the octahedra, which can be neglected in the non-Jahn-Teller compound $AFeO_3$, might be responsible for the slight differences, in Fig. 12(d), between the scaled lattice parameters of the two families. This implies that the elongations of the TiO_6 octahedra in $YTiO_3$ induce a decrease in $c/\sqrt{2}$ by about 0.5 Å, accompanied by a smaller increase in b, by about 0.3 Å, and by no noticeable change in a. These conclusions, obtained using the scaled plot of Fig. 12(d), confirm those deduced from geometrical arguments in Sec. V C 1.

3. *Anomalous character of the c axis?*

When T is reduced, the decrease in c is slowing down as the ferromagnetic transition at T_C is approached, which ends by an upturn below T_C, where c increases with decreasing T [see Fig. 2(a)]. The behavior of the c axis contrasts with those of the a and b axes, whose variations are monotonic for $4<T<300$ K and are amplified below T_C [see Fig. 2(a)]. The distortion of the (a,b) plane results mainly from the $GdFeO_3$-type distortion, whose modifications also control the uniaxial pressure dependences of T_C and T_N for $\mathbf{p}\|\mathbf{a},\mathbf{b}$ (see Sec. V C). In Secs. V C 1 and V C 2, c was shown to be more sensitive than a and b to the elongations of the TiO_6 octahedra, possibly related to a Jahn-Teller effect. The sensitivity of c to the distortions of the octahedra may be related to the anomalous uniaxial pressure dependences of T_C and T_N for $\mathbf{p}\|\mathbf{c}$ (see Sec. V B) and also to the anomalous behavior of the c axis in the spectral weight transfers of the optical conductivity.[17] Our findings are in apparent contradiction to theories according to which the Jahn-Teller distortion is an essential prerequisite of ferromagnetism in $YTiO_3$.[4,5] Rather,

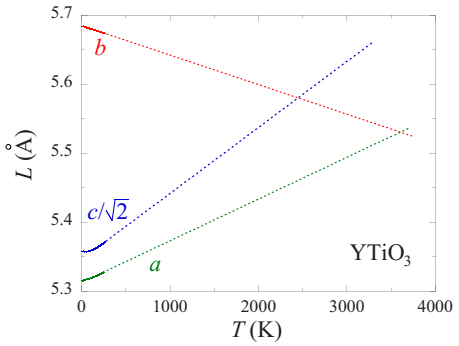

FIG. 13. (Color online) High-temperature linear extrapolation of the lattice parameters a, b, and $c/\sqrt{2}$ of $YTiO_3$.

the properties of $YTiO_3$ seem to be reminiscent of those of $La_{7/8}Sr_{1/8}MnO_3$, where a Jahn-Teller distortion is fully suppressed at the onset of ferromagnetism.[50]

D. High-temperature extrapolation

Equivalently to uniaxial pressures and variations of the A^{3+} ion size, increasing the temperature leads to a reduction in the distortion in the ABO_3 perovskites. Indeed, the strong anisotropy of the thermal expansion coefficients α_i, shown in Fig. 2(b), is governed by the effects of temperature on the crystal distortion. Assuming constant thermal expansion coefficients above room temperature, Fig. 13 shows high-temperature extrapolations, up to 4000 K, of the lattice parameters a, b, and $c/\sqrt{2}$.[51] This plot indicates that, in $YTiO_3$, a cubic structure with $a=b=c/\sqrt{2}$ (Ref. 43) might be recovered around 3000–4000 K. However, this temperature scale, characteristic of the lattice distortion, is inaccessible since it is far above the melting temperature of $YTiO_3$.

VI. CONCLUSION

The thermodynamic study of the perovskite system $YTiO_3$ presented here allowed us to extract information about the ferromagnetic ordering and its coupling to the lattice distortions. While the low-temperature specific-heat data, as well as an Arrott plot of the magnetization close to T_C, are consistent with a 3D Heisenberg picture of ferromagnetism, deviations from this simple picture were observed in the thermal expansion data at low temperature, where an unexpected power law is found. Above T_C, a magnetic signal persists up to the remarkably high temperature of $(5\pm1)T_C$. Further work is required to show whether models incorporating combined spin-orbital fluctuations, instead of spin-only fluctuations, could quantitatively describe this extended fluctuation regime.

Ehrenfest and Maxwell relations enabled us to extract the uniaxial pressure dependences of the Curie temperature T_C and of the spontaneous moment M_s, which indicates that ferromagnetism is stabilized by uniaxial pressures $\mathbf{p}\|\mathbf{a}$ and is destabilized by uniaxial pressures $\mathbf{p}\|\mathbf{b},\mathbf{c}$ and by hydrostatic pressure. We interpreted the uniaxial pressure dependences of T_C and M_s obtained for $\mathbf{p}\|\mathbf{a},\mathbf{b}$ as resulting from uniaxial pressure-induced modifications of the $GdFeO_3$-type distortion. A high sensitivity of the c axis to an additional distortion of the TiO_6 octahedra, possibly related to a Jahn-Teller effect, is believed to be responsible for the anomalous uniaxial pressure dependences of T_C and M_s observed for $\mathbf{p}\|\mathbf{c}$. This confirms that both kinds of distortion play an important role for the formation of ferromagnetism in $YTiO_3$, with the Jahn-Teller distortion being not a necessary condition for ferromagnetism in $YTiO_3$. While the a and b axes are more sensitive to the $GdFeO_3$-type distortion, the c axis is more sensitive to the elongations of the octahedra. Finally, a high-temperature extrapolation of the lattice parameters led to the onset of the distortion at a virtual temperature of about 3000–4000 K. These results might be considered to further develop models for the electronic properties of the titanates.

ACKNOWLEDGMENTS

We acknowledge useful discussions with T. Schwarz, D. Fuchs, M. Merz, R. Eder, O. Andersen, E. Pavarini, and G. Khaliullin. We thank K. Fischer for synthesizing the EuS crystal studied here. This work was supported by the Helmholtz-Gemeinschaft through the Virtual Institute of Research on Quantum Phase Transitions and Project VH-NG-016.

[1] J. B. Goodenough, Rep. Prog. Phys. **67**, 1915 (2004).
[2] J. P. Goral, J. E. Greedan, and D. A. Maclean, J. Solid State Chem. **43**, 244 (1982).
[3] Y. Okimoto, T. Katsufuji, Y. Okada, T. Arima, and Y. Tokura, Phys. Rev. B **51**, 9581 (1995).
[4] M. Mochizuki and M. Imada, New J. Phys. **6**, 154 (2004).
[5] E. Pavarini, A. Yamasaki, J. Nuss, and O. K. Andersen, New J. Phys. **7**, 188 (2005).
[6] A. C. Komarek, H. Roth, M. Cwik, W. D. Stein, J. Baier, M. Kriener, F. Bouree, T. Lorenz, and M. Braden, Phys. Rev. B **75**, 224402 (2007).
[7] J. Akimitsu, H. Ishikawa, N. Eguchi, T. Miyano, M. Nishi, and K. Kakurai, J. Phys. Soc. Jpn. **70**, 3475 (2001).
[8] F. Iga, M. Tsubota, M. Sawada, H. B. Huang, S. Kura, M. Takemura, K. Yaji, M. Nagira, A. Kimura, T. Jo, T. Takabatake, H. Namatame, and M. Taniguchi, Phys. Rev. Lett. **93**, 257207 (2004).
[9] I. V. Solovyev, Phys. Rev. B **74**, 054412 (2006).
[10] H. D. Zhou and J. B. Goodenough, Phys. Rev. B **71**, 184431 (2005).
[11] G. Khaliullin and S. Okamoto, Phys. Rev. B **68**, 205109 (2003).
[12] L. Craco, S. Leoni, and E. Müller-Hartmann, Phys. Rev. B **74**, 155128 (2006).
[13] S. Okatov, A. Poteryaev, and A. Lichtensein, Europhys. Lett. **70**, 499 (2005).
[14] C. Ulrich, G. Khaliullin, S. Okamoto, M. Reehuis, A. Ivanov, H.

He, Y. Taguchi, Y. Tokura, and B. Keimer, Phys. Rev. Lett. **89**, 167202 (2002).

[15] H. Maletta, J. Appl. Phys. **53**, 2185 (1982).

[16] H. Maletta and W. Zinn, in *Handbook of the Physics and Chemistry of Rare Earth*, edited by K. A. Gschneidner and L. Eyring (Elsevier, New York, 1989), Vol. 12, p. 213.

[17] N. N. Kovaleva, A. V. Boris, P. Yordanov, A. Maljuk, E. Bruchner, J. Strempfer, M. Konuma, I. Zegkinoglou, C. Bernhard, A. M. Stoneham, and B. Keimer, Phys. Rev. B **76**, 155125 (2007).

[18] C. Meingast, B. Blank, H. Bürkle, B. Obst, T. Wolf, H. Wühl, V. Selvamanickam, and K. Salama, Phys. Rev. B **41**, 11299 (1990).

[19] R. Pott and R. Schefzyk, J. Phys. E **16**, 444 (1983).

[20] U. Köbler and K. J. Fischer, Z. Phys. B **20**, 391 (1975).

[21] M. Tsubota, F. Iga, T. Takabatake, N. Kikugawa, T. Suzuki, I. Oguro, H. Kawanaka, and H. Bando, Physica B **281-282**, 622 (2000).

[22] J. D. Garrett, J. E. Greedan, and D. A. Maclean, Mater. Res. Bull. **16**, 145 (1981).

[23] N. Tsuji, M. Ito, H. Sakurai, K. Suzuki, K. Tanaka, K. Kitani, H. Adachi, H. Kawata, A. Koizumi, H. Nakao, Y. Murakami, Y. Taguchi, and Y. Tokura, J. Phys. Soc. Jpn. **77**, 023705 (2008).

[24] Well below the ordering temperature, ungapped ferromagnetic spin waves should lead to a T^d contribution to the specific heat and thermal expansion, while ungapped antiferromagnetic spin waves should lead to a $T^{d/2}$ contribution (d is the dimensionality of exchange). If there were the two kinds of branches in the low-energy excitations (strong ferromagnetic and weak antiferromagnetic-like spin waves), then two kinds of contributions should be present in both the specific heat and thermal expansion. In this case, the ferromagnetic contribution should dominate the specific heat because it has a higher intensity. Since the thermal expansion is related to the pressure dependence of the entropy, it is dominated by the most pressure-dependent energy scales. This means that weak antiferromagneticlike spin waves could dominate the low-temperature thermal expansion if they were associated with a strongly pressure-dependent energy scale.

[25] A. Arrott and J. E. Noakes, Phys. Rev. Lett. **19**, 786 (1967).

[26] In a limit with no domain effect and with $H \rightarrow 0$, Eq. (1) implies that $M=(T_C-T)^{\beta}$ for $T<T_C$ and $\chi=(T-T_C)^{-\gamma}$ for $T>T_C$.

[27] M. F. Collins, *Magnetic Critical Scattering* (Oxford University Press, New York, 1989).

[28] J.-G. Cheng, Y. Sui, J.-S. Zhou, J. B. Goodenough, and W. H. Su, Phys. Rev. Lett. **101**, 087205 (2008).

[29] W. Knafo, C. Meingast, S. Sakarya, N. H. van Dijk, Y. Huang, H. Rakoto, J.-M. Broto, and H. v. Löhneysen, arXiv:0807.4411, J. Phys. Soc. Jpn. (to be published).

[30] K. P. Belov, Fiz. Met. Metalloved. **2**, 447 (1956).

[31] For symmetry reasons, the thermal expansion coefficient α of a cubic system does not depend on the direction of the measured length L from which it is derived.

[32] A. Kornblit, G. Ahlers, and E. Buehler, Phys. Rev. B **17**, 282 (1978).

[33] J. Wosnitza and H. v. Löhneysen, Europhys. Lett. **10**, 381 (1989).

[34] P. Böni, M. Hennion, and J. L. Martínez, Phys. Rev. B **52**, 10142 (1995).

[35] P. Bloembergen, Physica B & C **85**, 51 (1977).

[36] W. Knafo, C. Meingast, K. Grube, S. Drobnik, P. Popovich, P. Schweiss, P. Adelmann, Th. Wolf, and H. v. Löhneysen, Phys. Rev. Lett. **99**, 137206 (2007).

[37] W. Knafo, C. Meingast, A. Inaba, Th. Wolf, and H. v. Löhneysen, J. Phys.: Condens. Matter **20**, 335208 (2008).

[38] C. Ulrich, A. Gössling, M. Grüninger, M. Guennou, H. Roth, M. Cwik, T. Lorenz, G. Khaliullin, and B. Keimer, Phys. Rev. Lett. **97**, 157401 (2006).

[39] C. Ulrich, G. Ghiringhelli, A. Piazzalunga, L. Braicovich, N. B. Brookes, H. Roth, T. Lorenz, and B. Keimer, Phys. Rev. B **77**, 113102 (2008).

[40] J. Hemberger, H. A. Krug von Nidda, V. Fritsch, J. Deisenhofer, S. Lobina, T. Rudolf, P. Lunkenheimer, F. Lichtenberg, A. Loidl, D. Bruns, and B. Buchner, Phys. Rev. Lett. **91**, 066403 (2003).

[41] T. Moriya and T. Takimoto, J. Phys. Soc. Jpn. **64**, 960 (1995).

[42] Y. Takahashi and T. Kanomata, Mater. Trans. **47**, 460 (2006).

[43] In an undistorted perovskite structure, the lattice parameters a, b, and c of the orthorhombic unit cell are related to the lattice parameter a_0 of the cubic unit cell by $a=b=c/\sqrt{2}=a_0\sqrt{2}$.

[44] D. du Boulay, E. N. Maslen, V. A. Streltsov, and N. Ishizawa, Acta Crystallogr., Sect. B: Struct. Sci. **51**, 921 (1995).

[45] In $YTiO_3$, elongations by 3% of the octahedra were explained by a Jahn-Teller effect in Refs. 4, 5, 7, and 8. In the non-Jahn-Teller $LaFeO_3$ and $YFeO_3$, but also in $LaTiO_3$, elongations, by about 1%, were reported in Refs. 6, 44, and 46 and are presumably consequences from the $GdFeO_3$-type distortion.

[46] J.-S. Zhou and J. B. Goodenough, Phys. Rev. B **77**, 132104 (2008).

[47] D. A. MacLean, H.-N. Ng, and J. E. Greedan, J. Solid State Chem. **30**, 35 (1979).

[48] M. Marezio, J. P. Remeika, and P. D. Dernier, Acta Crystallogr., Sect. B: Struct. Crystallogr. Cryst. Chem. **26**, 2008 (1970).

[49] R. D. Shannon, Acta Crystallogr., Sect. A: Cryst. Phys., Diffr., Theor. Gen. Crystallogr. **32**, 751 (1976).

[50] J. Geck, P. Wochner, S. Kiele, R. Klingeler, A. Revcolevschi, M. v. Zimmermann, B. Büchner, and P. Reutler, New J. Phys. **6**, 152 (2004).

[51] $i=i_0(1+\Delta L_i/L_i)$ where $i=a,b,c$ [cf. Fig. 2(a)] and where $a_0=5.331$, $b_0=5.672$, and $c_0=7.602$ Å were extracted from diffraction measurements at room temperature (Ref. 17).